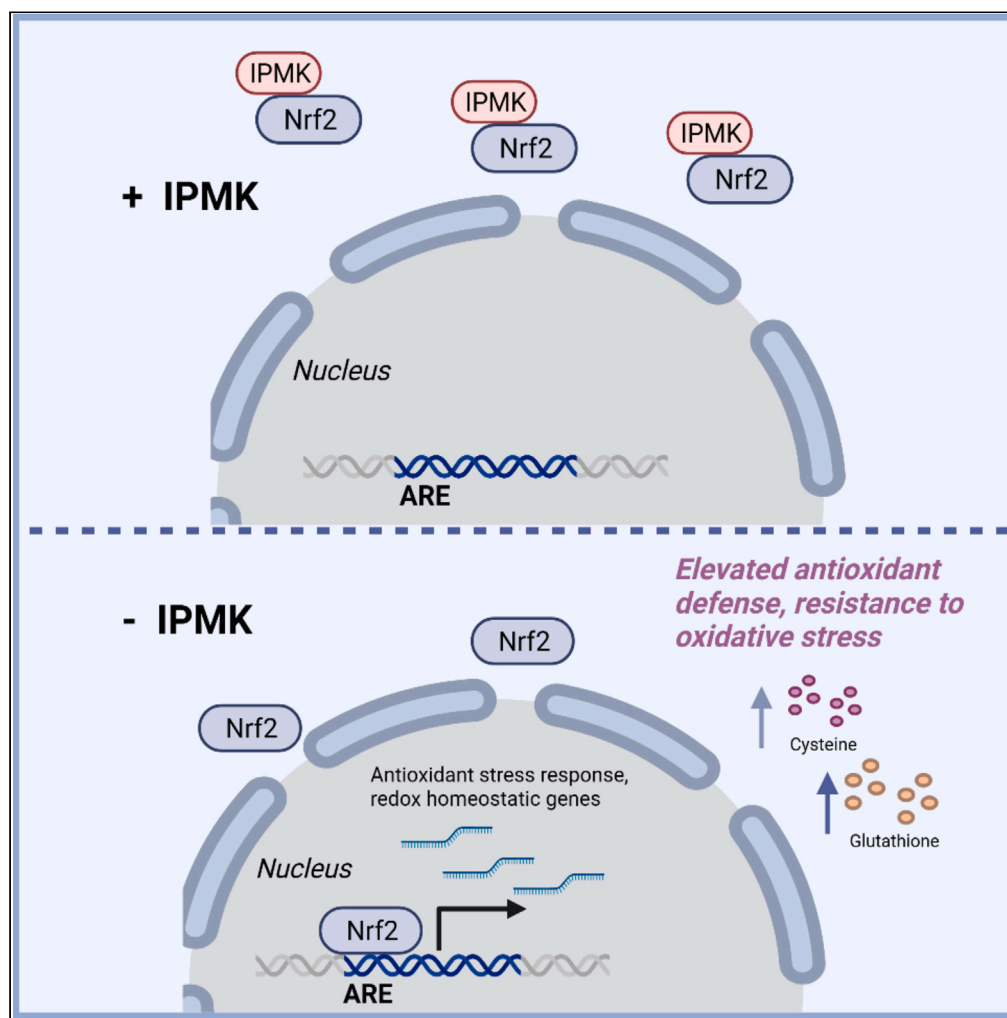**Article**

Inositol polyphosphate multikinase modulates redox signaling through nuclear factor erythroid 2-related factor 2 and glutathione metabolism

Richa Tyagi, Suwarna Chakraborty, Sunil Jamuna Tripathi, Ik-Rak Jung, Sangwon F. Kim, Solomon H. Snyder, Bindu D. Paul

bpaul8@jhmi.edu

Highlights

Depletion of IPMK confers resistance to oxidative stress

IPMK inhibits Nrf2, the master regulator of oxidative stress response

IPMK represses Nrf2 signaling independent of its catalytic activity

This study uncovers a new role for IPMK in modulating redox homeostasis in cells

Article

Inositol polyphosphate multikinase modulates redox signaling through nuclear factor erythroid 2-related factor 2 and glutathione metabolism

Richa Tyagi,[1,6] Suwarna Chakraborty,[2,6] Sunil Jamuna Tripathi,[2] Ik-Rak Jung,[3] Sangwon F. Kim,[1,3] Solomon H. Snyder,[1,2,4] and Bindu D. Paul[1,2,4,5,7,]*

SUMMARY

Maintenance of redox balance plays central roles in a plethora of signaling processes. Although physiological levels of reactive oxygen and nitrogen species are crucial for functioning of certain signaling pathways, excessive production of free radicals and oxidants can damage cell components. The nuclear factor erythroid 2-related factor 2 (Nrf2) signaling cascade is the key pathway that mediates cellular response to oxidative stress. It is controlled at multiple levels, which serve to maintain redox homeostasis within cells. We show here that inositol polyphosphate multikinase (IPMK) is a modulator of Nrf2 signaling. IPMK binds Nrf2 and attenuates activation and expression of Nrf2 target genes. Furthermore, depletion of IPMK leads to elevated glutathione and cysteine levels, resulting in increased resistance to oxidants. Accordingly, targeting IPMK may restore redox balance under conditions of cysteine and glutathione insufficiency.

INTRODUCTION

Inositol polyphosphates (IPs) are second messenger molecules that regulate a diverse array of physiologic processes, ranging from transcriptional regulation to vascular functions.[1,2] Inositols are a large family of molecules, broadly classified as water-soluble IPs or lipid inositols (phosphatidylinositols or phosphoinositides (PIPs)). These molecules are derivatives of myo-inositol, the most abundant stereoisomer of inositol, a six-carbon cyclic compound, which can be phosphorylated in various combinations to yield various IPs. Amongst the enzymes that generate higher order IPs, inositol polyphosphate multikinase (IPMK) is a key enzyme in the inositol polyphosphate biosynthetic pathway and catalyzes the rate-limiting step. IPMK is vital for embryogenesis with its deletion leading to multiple developmental defects and death at embryonic day 9.5.[3] IPMK sequentially phosphorylates inositol 1,4,5-triphosphate (IP_3) at positions 3 and 6, to generate inositol tetrakisphosphate (IP_4) and inositol pentakisphosphate (IP_5)[4] (Figure 1A).

IP_5 is utilized for the generation of the higher inositol polyphosphate species such as IP_6 and IP_7, which play multiple roles *in vivo.*[4–9] IP_7 can be further phosphorylated to form 1,5-IP_8 in cells.[10] IPMK also functions as a lipid kinase or phosphatidylinositol 3-kinase (PI3K), responsible for generating the bulk of phosphatidylinositol 3,4,5-triphosphate (PIP_3) from phosphatidylinositol (4,5)-bisphosphate (PIP_2).[11,12] PIP_3 is a second messenger that promotes cell proliferation, growth, and survival.[13] Besides its phosphatidylinositol 3-kinase activity, IPMK interacts with several target proteins to modulate various aspects of cellular physiology in an activity-independent manner.[14–18] IPMK plays important roles in transcriptional regulatory processes that govern signaling in diverse cell types. Its identification as a transcriptional regulatory protein preceded the discovery of its inositol kinase activity by almost two decades. Subsequently, its role in gene regulatory processes has begun to be more well-studied. IPMK acts as a coactivator for tumor-suppressor protein p53-induced apoptosis by stimulating its acetylation by p300 in a catalytic activity independent manner.[14] IPMK also functions as a coactivator in the induction of immediate-early genes for serum responsive factor (SRF) and cAMP-response element binding protein (CREB).[15,19] In addition, IPMK interacts with the mammalian target of rapamycin (mTOR), stabilizing and enhancing the activity of the mTOR complex 1 (mTORC1) in a manner that does not require its catalytic activity.[17,20] IPMK also has roles in the innate immune system and in inflammatory processes.[21] Thus, IPMK has diverse functions, consistent with its designation as a multifunctional protein.[22] Dysregulated IPMK signaling has been observed during certain pathological conditions and in neurodegenerative diseases such as Huntington's disease (HD).[23,24]

[1]The Solomon H. Snyder Department of Neuroscience, Johns Hopkins University School of Medicine, Baltimore, MD 21205, USA

[2]Department of Pharmacology and Molecular Sciences, Johns Hopkins University School of Medicine, Baltimore, MD 21205, USA

[3]Division of Endocrinology, Diabetes, and Metabolism, Department of Medicine, Johns Hopkins University, Baltimore, MD 21224, USA

[4]Department of Psychiatry and Behavioral Sciences, Johns Hopkins University School of Medicine, Baltimore, MD 21205, USA

[5]Lieber Institute for Brain Development, Baltimore, MD 21205, USA

[6]These authors contributed equally

[7]Lead contact

*Correspondence: bpaul8@jhmi.edu

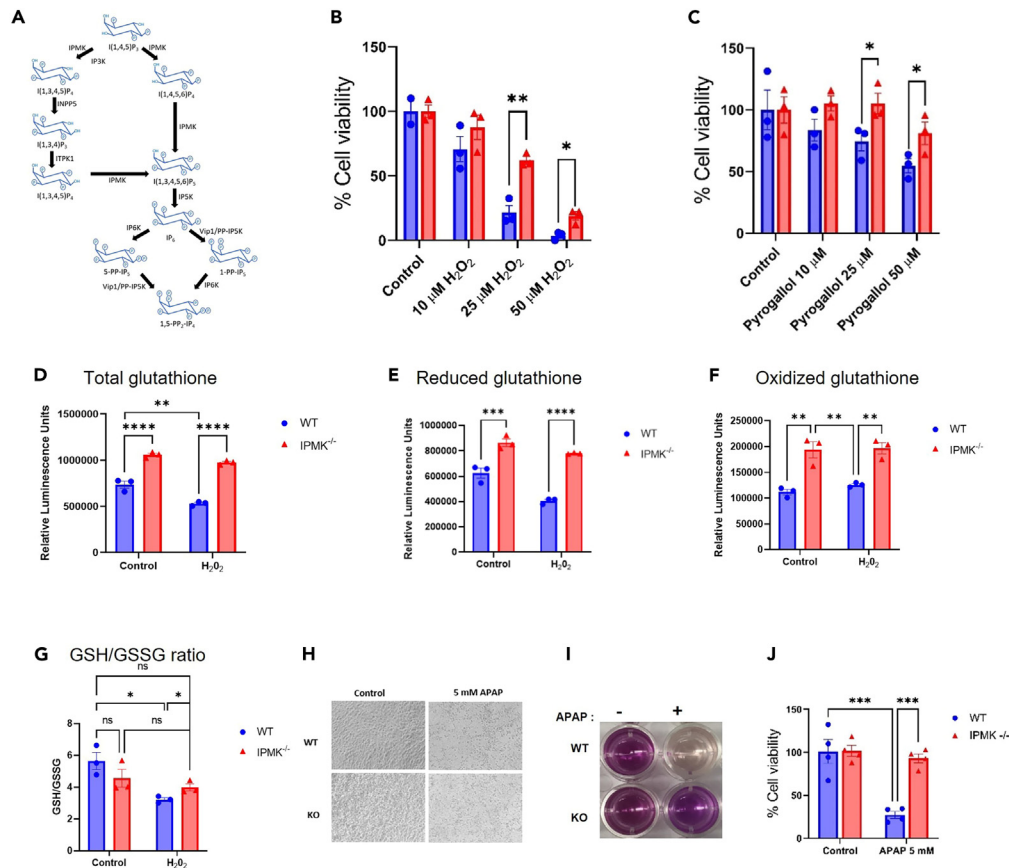https://doi.org/10.1016/j.isci. 2023.107199

Figure 1. Cells lacking inositol polyphosphate multikinase (IPMK) exhibit increased resistance to oxidative stress

(A) The inositol phosphate biosynthetic pathway. IPMK phosphorylates inositol 1,4,5-triphosphate (IP3) sequentially at positions 3 and 6, to generate inositol tetrakisphosphate (IP4) and inositol pentakisphosphate (IP5). IP5 is further acted on by IP5K to yield IP6. IP6 is acted on by IP6 kinases (IP6Ks) pyrophosphorylating the 5 position, to produce 5-PP-IP4 from IP5, 5-PP-IP5 (5-IP7) from IP6, and 1-5-(PP)2-IP4 (1,5-IP8) from IP7. PP-IP5Ks, which are the human Vip1 isoforms, pyrophosphorylate the 1 or 3 position to generate 1-IP7 from IP6, or 1,5-IP8 from 5-IP7. DIPPs are the dephosphorylating enzymes which convert inositol pyrophosphates to IP6 or IP5.

(B) IPMK deleted cells exhibit increased resistance to cell death induced by H_2O_2. Wild-type and $IPMK^{-/-}$ MEFs were treated with increasing concentrations of H_2O_2 for 24 h and cell viability assessed by the 3-(4,5-dimethylthiazol-2-yl)-2,5-diphenyltetrazolium bromide (MTT) assay. **$p < 0.01$, *$p < 0.05$, two-way ANOVA followed by Tukey's post hoc test (n = 2–3, mean ± SEM).

(C) IPMK deleted cells exhibit increased resistance to cell death induced by pyrogallol. Wild-type and $IPMK^{-/-}$ MEFs were treated with increasing concentration of the superoxide generator, pyrogallol, and viability measured as described in B. **$p < 0.01$, ****$p < 0.0001$, two-way ANOVA followed by Tukey's post hoc test (n = 3, mean ± SEM).

(D–F) Glutathione (GSH) levels are higher in cells lacking IPMK. Cells were treated with 25 μM H_2O_2 for 24 h and GSH levels measured. **$p < 0.01$, ****$p < 0.0001$, two-way ANOVA followed by Tukey's post hoc test (n = 3, mean ± SEM).

(G) Glutathione levels are higher in $IPMK^{-/-}$ MEFs, which include the total, reduced and oxidized levels. GSH/GSSG ratio in both cell types are not significantly different under basal conditions, but in response to H_2O_2 treatment, the $IPMK^{-/-}$ MEFs have a higher GSH/GSSG ratio as compared to the wild-type. **$p < 0.01$, ****$p < 0.0001$, two-way ANOVA followed by Tukey's post hoc and test (n = 3, mean ± SEM).

(H–J) IPMK knockout cells are resistant to toxicity induced by acetaminophen (APAP). Cells were treated with 5 mM APAP, which depletes cellular GSH and decreases cell viability measured by the MTT assay. ***$p < 0.001$, two-way ANOVA followed by Tukey's post hoc test (n = 4, mean ± SEM).

Thus, physiological roles of IPMK and underlying molecular mechanisms are still being elucidated. In this study we identify the way IPMK modulates redox balance in cells. Here, we report that IPMK is a negative regulator of cellular redox signaling and depletion of IPMK leads to increased resistance to oxidative stress. We uncover new roles for IPMK as a modulator of signaling mediated by nuclear factor erythroid 2-related factor 2 (Nrf2), the master regulator of redox balance and antioxidant stress responses in cells.

RESULTS

Loss of IPMK confers increased resistance to oxidative stress

As IPMK deletion is embryonic lethal, to elucidate the roles of IPMK in cellular signaling, we utilized IPMK knockout mouse embryonic fibroblast (MEF) cell lines generated using the cre-lox targeting strategy.[3,12,14] To further examine the role of IPMK in stress responses, we analyzed the response of $IPMK^{-/-}$ MEFs to oxidative stress. We treated wild-type and $IPMK^{-/-}$ with oxidants such as hydrogen peroxide (H_2O_2) and pyrogallol (a superoxide generator) and an agent which depletes glutathione (GSH) and monitored their survival using the 3-(4,5-dimethylthiazol-2-yl)-2, 5-diphenyltetrazolium bromide (MTT) assay. Treatment of these cells with increasing concentrations of H_2O_2 revealed that the $IPMK^{-/-}$ MEFs were more resistant to cell death induced by H_2O_2 (Figure 1B). At 25 μM H_2O_2, the viability of wild-type cells was approximately 20%, whereas that of the $IPMK^{-/-}$ MEFs was approximately 60%. Similarly, treatment with pyrogallol revealed that $IPMK^{-/-}$ MEFs were more resistant to cell death (Figure 1C). As GSH plays a central role in redox balance, we further studied the effects of IPMK depletion on GSH levels, we quantitated the levels of glutathione in wild-type and $IPMK^{-/-}$ MEFs. As GSH is an abundant antioxidant in cells, its depletion causes increased oxidative stress.[25,26] The $IPMK^{-/-}$ MEFs have elevated levels of total GSH, reduced as well as oxidized GSH (GSSG), which could account for the increased resistance to oxidative stress (Figures 1D–1G). Although the GSH/GSSG ratio was not significantly different in the wild-type and $IPMK^{-/-}$ MEFs during basal conditions, the GSH/GSSG in wild-type cells showed a greater decrease with H_2O_2 as compared to the $IPMK^{-/-}$ MEFs, indicating that the $IPMK^{-/-}$ have a more reducing environment with respect to glutathione homeostasis (Figure 1G). Next, we depleted the cellular GSH in cells using acetaminophen (APAP), a commonly used analgesic and antipyretic (also known as paracetamol). APAP toxicity is caused by its highly reactive metabolite, N-acetyl-p-benzoquinone imine (NAPQI), which is detoxified by reduced glutathione.[27–29] To study the effect of IPMK deletion on sensitivity to APAP, $IPMK^{-/-}$ MEFs and their wild-type controls were treated with APAP (5 mM) for 18 h and cell viability assessed using the 3-(4, 5-dimethylthiazol-2-yl)-2, 5-diphenyltetrazolium bromide (MTT) assay. The $IPMK^{-/-}$ MEFs were more resistant to toxicity induced by APAP and exhibited a higher survival rate as compared to wild-type cells (Figures 1H–1J).

IPMK depleted cells have elevated cysteine levels

GSH (L-gamma-glutamyl-L-cysteinylglycine), is a tripeptide composed of glycine, cysteine and glutamate, with the availability of cysteine being the rate limiting step for its biosynthesis.[30] As cysteine has antioxidant activities itself, we studied its disposition in the $IPMK^{-/-}$ MEFs. Cysteine, a semi-essential amino acid can be produced endogenously as well through the transsulfuration pathway from homocysteine, which in turn is generated from dietary methionine[31,32] (Figure 2A). Cystathionine γ-lyase (CSE), a key enzyme in the transsulfuration pathway, is the biosynthetic enzyme for cysteine, generating it from cystathionine. The cysteine is then acted on by γ-glutamyl cysteine synthetase (γ-GCS) and glutathione synthetase (GS) to produce GSH. To analyze whether cysteine metabolism is altered in the $IPMK^{-/-}$ MEFs, we measured the production of cysteine in the $IPMK^{-/-}$ MEFs using the ninhydrin assay.[33] In these experiments, the wild-type and $IPMK^{-/-}$ MEFs were seeded to have equal cell numbers. Cysteine levels were increased almost two-fold in cells lacking IPMK (Figure 2B). In addition, these cells survived better in cell culture when cysteine was depleted (0.05 mM cysteine) from the growth medium indicative of their increased capacity for cysteine biosynthesis (Figures 2C and 2D). Cell viability was also assessed using propidium iodide staining and trypan blue staining, which further confirmed the observation that $IPMK^{-/-}$ MEFs displayed increased survival in low cysteine medium as compared to wild-type MEFs (Figures S1A and S1B). To further validate the effect of IPMK on growth during cysteine starvation, we utilized $IPMK^{-/-}$ cells complemented with wild-type IPMK. Similar to the wild-type cells, IPMK null cells complemented with IPMK also exhibited reduced survival during total cysteine deprivation (Figure 2E).

Cysteine, a semi-essential amino acid, is imported into cells as well as generated *de novo* from dietary methionine.[31] Cystine, the oxidized form of cysteine, is taken up by system x_c^- in a Na+-independent but chloride dependent manner. The x_c^- transporter is a heterodimer of light (xCT/SLC7A11) and heavy chains (4F2hc/CD98/SLC3A2), where the xCT subunit confers substrate specificity.[34,35] xCT is induced in response to a variety of stimuli including oxidative stress, inflammation and electrophilic compounds.[36,37] Inhibiting xCT triggers oxidative stress by preventing the import of cystine and decreasing GSH biosynthesis. We treated wild-type and $IPMK^{-/-}$ MEFs with sulfasalazine (SSZ), an xCT inhibitor for 18 h and assessed cell viability. Similar to the response to APAP, cell death induced by SSZ was more pronounced in the wild-type cells as compared to the IPMK deleted cells (Figure 2F). We also depleted cysteine in cells
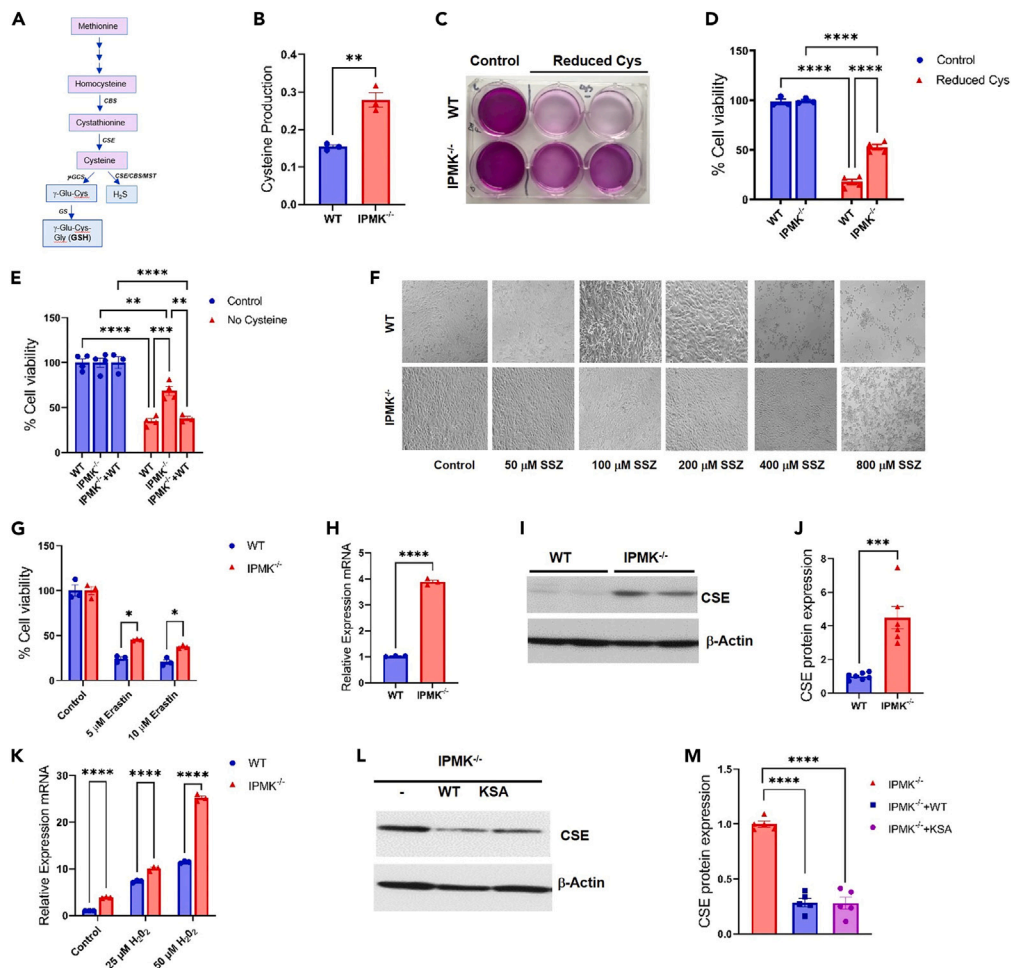
Figure 2. IPMK knockout cells exhibit compromised cysteine metabolism

(A) The reverse transsulfuration pathway via which cysteine and GSH are produced. Homocysteine, derived from dietary methionine is converted to cystathionine by cystathionine β-synthase (CBS), which is then acted on by cystathionine γ-lyase (CSE) to produce cysteine. Cysteine can then be channelized to produce the antioxidant GSH. Cysteine and homocysteine may also be utilized by CSE and CBS to produce the gaseous signaling molecule, hydrogen sulfide (H_2S).

(B) Cysteine production in $IPMK^{-/-}$ MEFs. The generation of cysteine from cystathionine was measured by the ninhydrin assay, which revealed an increased capacity of $IPMK^{-/-}$ cells to produce cysteine. **$p < 0.01$, Two-tailed Student's t test (n = 3, mean ± SEM).

(C) Growth of cells in a 6-well plate in low cysteine medium. $IPMK^{-/-}$ MEFs were plated in growth medium with low cysteine. Compared to wild-type cells, $IPMK^{-/-}$ cells survive better in low cysteine medium (0.05 mM).

(D) Viability of $IPMK^{-/-}$ MEFs and their wild-type controls in reduced cysteine medium, as revealed by the 3-(4,5-dimethylthiazol-2-yl)-2,5-diphenyltetrazolium bromide (MTT) assay. ****$p < 0.0001$, two-way ANOVA followed by Tukey's post hoc test (n = 3–4, mean ± SEM).

(E) Complementing $IPMK^{-/-}$ MEFs with IPMK decreases viability during total cysteine starvation. Wild-type, $IPMK^{-/-}$ and $IPMK^{-/-}$ cells complemented with IPMK were grown either in regular or zero cysteine medium and viability assessed by the MTT assay. **$p < 0.01$, ***$p < 0.001$, ****$p < 0.0001$. two-way ANOVA followed by Tukey's post hoc test (n = 3–4, mean ± SEM).

(F) $IPMK^{-/-}$ MEFs survive better in medium containing sulfasalazine (SSZ). Cells were treated with increasing concentrations of SSZ, an inhibitor of the cystine transporter protein, xCT, to deplete cysteine intracellularly overnight for 18 h and viability monitored.

(G) $IPMK^{-/-}$ MEFs survive better in medium containing erastin. Cells were treated with increasing concentrations of erastin, an inhibitor of the cystine transporter protein, xCT, to deplete cysteine intracellularly overnight for 18 h and viability monitored. *$p < 0.05$, two-way ANOVA followed by Tukey's post hoc test (n = 3, mean ± SEM).

(H) Transcript levels of CSE in wild-type and $IPMK^{-/-}$ cells. ****$p < 0.0001$, Two-tailed Student's t test (n = 3, mean ± SEM).

(I) Levels of CSE protein (left) are upregulated in $IPMK^{-/-}$ cells as revealed by western blotting.

(J) Quantitation of (I). ****$p < 0.0001$, Two-tailed Student's t test (n = 6–7, mean ± SEM).

Figure 2. *Continued*

(K) Induction of CSE transcripts in response to oxidative stress. Cells were treated with increasing concentrations of H_2O_2 for 24 h and total RNA isolated. Transcript levels of CSE were quantitated by qPCR. ****$p < 0.0001$, two-way ANOVA followed by Tukey's post hoc test (n = 3, mean ± SEM).

(L) IPMK represses CSE expression. IPMK knockout mouse embryonic fibroblasts were stably transfected with either wild type IPMK, the catalytically inactive KSA mutant of IPMK and expression of CSE observed. Both the wild type and mutant IPMKs decreased expression of CSE. ****$p < 0.0001$, One-way ANOVA followed by Tukey's post hoc test (n = 3, mean ± SEM).

(M) Quantitation of (L). ****$p < 0.0001$, One-way ANOVA followed by Tukey's post hoc test (n = 5, mean ± SEM).

by treating them with erastin, an inhibitor of xCT. Once again, the IPMK-deleted cells survived better under these conditions (Figure 2G). As cysteine can be generated by cells, we analyzed the abundance of CSE, its biosynthetic enzyme, both at the protein and transcript levels. CSE was highly upregulated in the $IPMK^{-/-}$ MEFs both at the mRNA and protein levels (Figures 2H–2J). CSE (*Cth*) is increased approximately 2-fold at the mRNA level and by more than 5-fold at the protein level. As cysteine and GSH play vital roles in the maintenance of redox balance in cells, we further characterized the oxidative stress response in IPMK-depleted cells. We treated wild-type and $IPMK^{-/-}$ MEFs with H_2O_2 and monitored expression of CSE, which is induced in response to oxidative stress.[38] Consistent with our observations, CSE was induced in both cell types, however the basal and induced expression of CSE was much higher in $IPMK^{-/-}$ MEFs (Figure 2K). To ascertain whether the catalytic activity of IPMK influences CSE expression, we complemented $IPMK^{-/-}$ MEFs with wild-type and catalytically dead IPMK and analyzed levels of CSE at the protein level. Both wild-type as well as catalytically inactive IPMK (KSA, IPMK K129A/S235A) downregulated the expression of CSE (Figures 2L and 2M). Taken together, our findings suggest that IPMK is a negative regulator of cysteine and GSH metabolism in an activity-independent manner.

IPMK depletion enhances oxidative stress response in cells

We next asked the question -whether IPMK might modulate the oxidative stress response in general. Toward this end, we analyzed the expression of other genes which maintain redox balance in cells. We isolated RNA from wild-type and $IPMK^{-/-}$ cells and analyzed the expression of genes involved in antioxidant defense using a pathway-focused PCR array. (Figure 3A). Consistent with our observation that the antioxidant defense mechanisms are boosted in $IPMK^{-/-}$ cells, we observed an upregulation of genes involved in glutathione metabolism and redox homeostasis such as glutamate cysteine ligase catalytic subunit/γ-glutamylcysteine synthetase subunit (*Gclc*), glutamate cysteine ligase modifier subunit (*Gclm*), ferritin heavy chain 1 (*Fth1*) and superoxide dismutase 3 (*Sod3*) (Figure 3A). A closer inspection of the upregulated genes revealed that several of these genes were direct targets of the nuclear factor erythroid 2-related factor 2 (Nrf2), the master regulator of redox homeostasis and detoxification pathways (Figure 3B).[39–41] We further validated the upregulation of genes regulated by Nrf2 by quantitative RT-PCR (qRT-PCR) using wild-type and $IPMK^{-/-}$ MEFs. The expression of *Fth1*, *Gclc, Gclm,* glutathione peroxidase 1 (*Gpx1*), glutathione peroxidase 7 (*Gpx7*), glutathione S-transferase A2 (*GstA2*), heme oxygenase 1 (*Hmox1*), NADPH quinone oxidoreductase 1 (*Nqo1*), phosphoglucono dehydrogenase (*Pgd*), peroxiredoxin 2 (*Prdx2*) and thioredoxin reductase 1 (*Txnrd1*) were upregulated in $IPMK^{-/-}$ MEFs (Figures 3C–3M).The expression of some of these genes was also tested at the protein level. Nqo1, Gclc, Txnrd1, Pgd, Gpx1/2, and Prdx2 were upregulated at the protein level too, confirming the upregulation of the Nrf2 signaling (Figure 3N). To determine whether these changes occurred *in vivo* as well, we utilized liver-specific knockouts of IPMK as whole-body knockouts are embryonic lethal. qRT-PCR of total RNA isolated from the liver of wild-type and liver-specific knockouts of IPMK revealed an upregulation of Nrf2 target genes, confirming our observations in cell culture models of IPMK depletion (Figures S2A–S2F).

Thus, IPMK modulates the Nrf2 signaling pathway to influence redox homeostasis in cells, establishing a link between the inositol signaling molecules and glutathione metabolism. Deletion of IPMK results in increased levels of GSH and an upregulation of antioxidant defense mechanisms. GSH is the most abundant antioxidant in cells and is utilized in a plethora of reactions either as a cofactor or as a reducing agent. GSH participates in multiple pathways, which include those involved in detoxification pathways and antioxidant defense.[42] Levels of cysteine, a component of GSH which is a tripeptide comprising glycine, glutamate and cysteine, are also increased in $IPMK^{-/-}$ cells. The biosynthesis as well as uptake of cysteine and cystine are tuned up in these cells, translating to increased GSH biosynthesis and resistance to oxidative stress. The levels of CSE are upregulated significantly in $IPMK^{-/-}$ cells which result in increased cysteine and GSH biosynthesis. The upregulation of the transsulfuration pathway has been observed in several
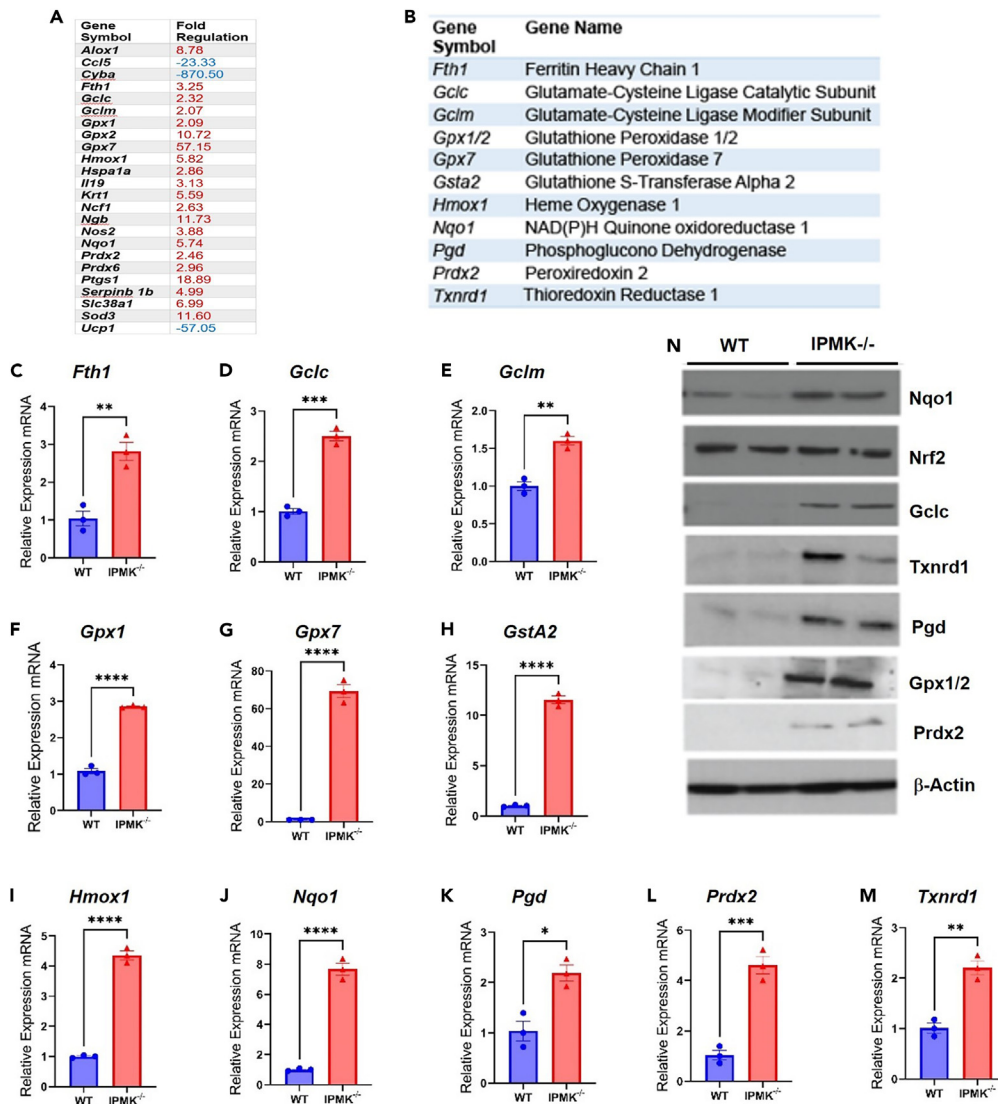
A

Gene Symbol	Fold Regulation
Alox1	8.78
Ccl5	-23.33
Cyba	-870.50
Fth1	3.25
Gclc	2.32
Gclm	2.07
Gpx1	2.09
Gpx2	10.72
Gpx7	57.15
Hmox1	5.82
Hspa1a	2.86
Il19	3.13
Krt1	5.59
Ncf1	2.63
Ngb	11.73
Nos2	3.88
Nqo1	5.74
Prdx2	2.46
Prdx6	2.96
Ptgs1	18.89
Serpinb 1b	4.99
Slc38a1	6.99
Sod3	11.60
Ucp1	-57.05

B

Gene Symbol	Gene Name
Fth1	Ferritin Heavy Chain 1
Gclc	Glutamate-Cysteine Ligase Catalytic Subunit
Gclm	Glutamate-Cysteine Ligase Modifier Subunit
Gpx1/2	Glutathione Peroxidase 1/2
Gpx7	Glutathione Peroxidase 7
Gsta2	Glutathione S-Transferase Alpha 2
Hmox1	Heme Oxygenase 1
Nqo1	NAD(P)H Quinone oxidoreductase 1
Pgd	Phosphoglucono Dehydrogenase
Prdx2	Peroxiredoxin 2
Txnrd1	Thioredoxin Reductase 1

Figure 3. IPMK deletion increases expression of oxidative stress response genes

(A) Genes on an oxidative stress response pathway focused PCR array that show differential expression in IPMK knockout cells.

(B) Genes on the PCR array regulated by nuclear factor erythroid 2-related factor 2 (Nrf2).

(C–M) Validation of differential expression of genes (*Fth1, Gclc, Gclm, Gpx1, Gpx7, GstA2, Hmox1, Nqo1, Pgd, Prdx2* and *Txnrd1*) regulated by Nrf2 by quantitative RT-PCR. *$p < 0.05$, **$p < 0.01$, ***$p < 0.001$, ****$p < 0.0001$. Two-tailed Student's t test (n = 3, mean ± SEM).

(N) Expression of the oxidative stress response genes at the level of protein expression. (n = 3).

cancers and depleting cysteine restricts cancer growth.[43–45] In addition, the key enzyme of the GSH biosynthetic pathway, γ-glutamylcysteine synthetase (γ-GCS/GCLC), is upregulated in cells lacking IPMK.

Our findings tie together, several previously reported effects of IPMK, which can be attributed to the regulation of redox signaling involving cysteine and GSH metabolism, by IPMK. For instance, IPMK inhibits angiogenesis through its effects on the hypoxia inducible factor 1α (HIF1α) which regulates vascular endothelial growth factor (VEGF), a master regulator of vascular function.[46] On the other hand, CSE generates H₂S, which promotes angiogenesis and vascular function.[47–49] Thus, the elevated levels of CSE observed in cells lacking IPMK, may also participate in stimulating angiogenesis. Several effects of CSE are counteracted by IPMK. IPMK depletion has been associated with increased incidence of certain cancers, and one of

the reasons responsible for increased proliferation is increased GSH content, which is a characteristic feature of IPMK-depleted cells as elucidated by this study. IPMK has been reported to inhibit the activity of AMP-activated protein kinase (AMPK) and reciprocally increase mTOR activity by activating Akt.[17,50] CSE, which is upregulated when IPMK is depleted, on the other hand, activates AMPK.[51] Along a similar vein, AMPK activates the Nrf2 pathway, and we now show that IPMK inhibits this pathway. H_2S produced by CSE activates the Nrf2 pathway by promoting nuclear translocation of Nrf2.[52,53] Of note, quercetin and flavonoids inhibit IPMK activity and activate Nrf2 signaling.[54] Taken together, these findings underscore the ability of IPMK to modulate the antioxidant stress response pathways. The effect of IPMK on the transcription of antioxidant stress response genes is independent of its catalytic activity. This noncatalytic action of IPMK is also observed in the case of its influence on other transcriptional regulators such as p53 and serum response factor (SRF) and the yeast Arg82 protein.[14,15,18] Of interest, p53 has been reported to inhibit Nrf2 signaling, further linking this study to our prior studies involving p53 and IPMK.[55] The study of the interplay between IPMK, Nrf2 and p53 would provide additional insights into how these signaling pathways act in health and disease.

The Nrf2 signaling cascade is an evolutionarily conserved stress response pathway which protects against oxidative stress and xenobiotics.[56] Under basal conditions, Nrf2 is sequestered by Kelch-like ECH-associated-protein 1 (Keap1) and targeted for ubiquitination and degradation.[57,58] During oxidative stress, Nrf2 dissociates from Keap1, translocates to the nucleus and binds to promoters harboring the antioxidant response elements (AREs) and activates their transcription.[57,59] As Nrf2-target genes are upregulated in IPMK-deficient cells, we asked how IPMK might modulate Nrf2 signaling. In addition, we explored whether there was a direct link between IPMK and Nrf2. Accordingly, we conducted GST pulldown studies, which revealed that IPMK bound Nrf2 (Figure 4A). We further mapped the sites on IPMK that interact with Nrf2, using various deletion constructs of IPMK (Figure S3A). IPMK harbors both a nuclear export signal (NES) as well as a nuclear localization signal (NLS) and thus can shuttle between the nucleus and cytoplasm.[60] Some of its critical functions in cell growth and proliferation require cytoplasmic localization.[12,20] GST pulldown analysis revealed that Nrf2 interacted with the C-terminal end of IPMK, which is in close proximity to its NLS. The region of IPMK interacting with Nrf2 harbors the ATP binding site (Figure S3B). We also confirmed the endogenous interaction of IPMK in liver lysates and brain (cortex) lysates of wild-type C57BL/6J mice (Figures S3C and S3D). Next, we studied the subcellular localization of Nrf2 when IPMK was overexpressed in HEK293 cells. The presence of IPMK decreased nuclear levels of Nrf2, indicating that IPMK sequesters Nrf2 in the cytoplasm (Figure 4B). The subcellular distribution analysis revealed that the presence of IPMK decreased the nuclear localization of Nrf2 significantly (Figure 4C).

We further analyzed the expression of Nrf2-regulated genes at the level of proteins in wild-type, IPMK null cells and the IPMK null cells complemented with either wild-type IPMK or catalytically dead KSA mutant of IPMK. The expression of the Nrf2 targets, xCT, Gclc, GstA2, and HO-1 were increased in IPMK null cells, but not those that were complemented with either the wild-type or mutant IPMK, indicating that the catalytic activity of IPMK was not involved in the process (Figure 4D). This decrease in regulation of the Nrf2 genes tested, occurred at the transcriptional level as determined by the levels of the transcripts of these genes (Figures 4E–4H). Taken together, our results suggest that IPMK decreases nuclear localization of Nrf2 and diminishes expression of its target genes (Figure 4I).

DISCUSSION

In vivo significance of the links between IPMK and Nrf2 signaling

In summary, we have identified a role for IPMK in the control of redox balance in cells. Redox regulation involving cysteine and GSH metabolism plays vital roles in the maintenance of cellular function. GSH serves as a cofactor for numerous antioxidant response proteins such as peroxiredoxins and glutathione peroxidases. GSH also functions as a reducing factor for the generation of NADPH from NADP. In addition, GSH serves as a reservoir for synaptic glutamate, which participates in neurotransmission and regulation of long-term potentiation (LTP).[61] The GSH cycle molds the activity of synaptic glutamate, the major excitatory neurotransmitter in the central nervous system. The molecular mechanisms underlying complex neuropsychiatric diseases such as schizophrenia involve multiple dysregulated pathways including GSH disposition among others.[45,62–64] Inhibiting GCL, which utilizes glutamate to synthesize glutathione, leads to increased glutamate and neurotransmission, whereas decreasing the release of glutamate from the glutathione cycle by blocking γ-glutamyl transferase, which releases glutamate from GSH had the opposite effect. In this study, we have identified the interaction between one of the key signaling pathways that regulate redox
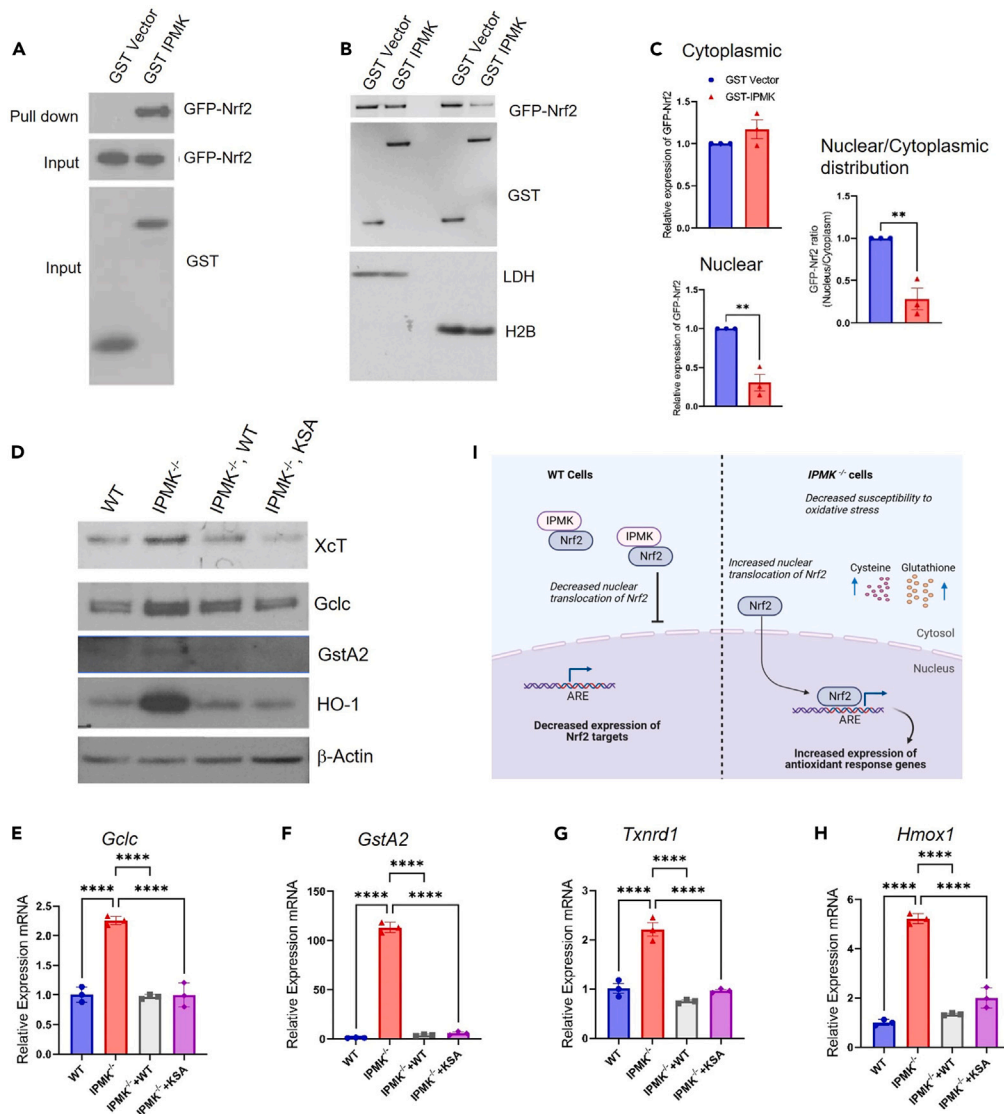
Figure 4. IPMK binds Nrf2 and inhibits its activity

(A) IPMK interacts with Nrf2. HEK293 cells were transfected with GFP-Nrf2 and either empty GST vector or GST-IPMK for 24 h, following which cells were harvested and GST-pulldown conducted using GSH Sepharose beads and analyzed by western blotting using anti-GFP Nrf2.

(B) Nuclear Nrf2 is decreased by IPMK. A representative western blot showing the distribution of GFP-Nrf2 in the nuclear and cytoplasmic compartment. HEK293 cells were transfected with GFP-Nrf2 and either empty GST vector or GST-IPMK for 24 h, following which cells were harvested and nuclear and cytoplasmic fractions analyzed for localization of Nrf2 by western blotting with anti-GFP antibodies. Anti-histone H2B (nuclear marker) and lactate dehydrogenase (LDH, cytoplasmic marker) were utilized to assess the purity of the samples. In the presence of IPMK, nuclear localization of GFP-Nrf2 is diminished.

(C) Quantitation of relative levels of GFP-Nrf2 in the nuclear and cytoplasmic compartments. **$p < 0.01$, Two-tailed Student's t test ($n = 3$, mean $\pm$ SEM).

(D) Catalytic activity of IPMK is not required for diminishing expression of Nrf2 targets. Lysates from wild-type MEFs, IPMK null cells and IPMK null cells complemented either with wild-type IPMK or catalytically inactive KSA mutant were prepared and expression of the Nrf2 targets analyzed. IPMK inhibited the expression of the tested Nrf2 target genes in a catalytically independent manner.

(E–H) The suppression of Nrf2 targets, *Gclc*, *GstA2*, *Hmox1* and *Txnrd1* occur at the transcriptional level. ****$p < 0.0001$, Two-tailed Student's t test ($n = 3$, mean $\pm$ SEM).

(I) Model depicting IPMK action. In wild-type cells, IPMK regulates Nrf2 activity by binding to it and inhibiting its nuclear translocation. As a result, when IPMK is depleted, increased nuclear translocation of Nrf2 occurs, leading to elevated expression of target genes.

balance and IPMK. Our findings unveil a functional intersection of conserved cellular pathways, namely, inositol signaling and antioxidant signaling cascades. Cells harbor a variety of such signaling pathways, which protect them from irreversible oxidative damage. These intersecting cascades may offer selective advantages in the overall adaptive strategy harnessed by cells to protect themselves against the damaging effects of stress stimuli. The fine-tuning of Nrf2 action by IPMK may represent one such mode of action. Aberrant Nrf2 signaling has been observed in premature aging, leading to redox imbalance.[65] Indeed, dysregulated cysteine and GSH metabolism is also a feature of several neurological diseases such as HD and restoring this balance is beneficial.[31,66–68] Redox imbalance is linked to immune system abnormalities and energy metabolism and plays a central role in the pathogenesis of emergent diseases such as COVID-19.[69] An avenue for future study could be the epigenetic effects of IPMK in modulating gene expression. Another interesting avenue of research involves role of dysregulated IPMK in development of certain cancers. Decreased expression of IPMK has been observed in certain cancers, such as the papillary thyroid cancer and overexpression of IPMK was beneficial, inhibiting the proliferation, migration, and invasion of PTC cells.[70] These findings align with our prior studies on IPMK is an activator of the tumor-suppressor protein p53.[14] Loss of p53 function is highly linked to several intestinal cancers. Of interest, Nrf2 signaling is activated in PTCs[71] and p53, which is activated by IPMK is known to antagonize Nrf2 signaling.[55] Thus, depletion of IPMK may diminish activity of p53 and cause tumorigenesis in a subset of cancers. Accordingly, detailed studies focused on IPMK and its role on various aspects of redox signal transduction cascades may unveil additional nodes of regulation, which may be targeted for therapeutic intervention in chronic neurodegenerative and neuropsychiatric diseases involving redox imbalance.

Limitations of the study

Our studies identify a link between the master regulator of redox homeostasis, Nrf2, and IPMK. In our study, the catalytic activity of IPMK was not necessary for its effects on the Nrf2 target genes tested, as revealed by the complementation studies. It is not clear whether IPMK functions in a manner similar to Keap1, which is a strong negative regulator of Nrf2, targeting it for ubiquitination. Nevertheless, our data strongly demonstrate the expression levels of IPMK affects the activation of Nrf2. Even though there have been numerous studies showing how IPMK contributes to the various signaling cascades utilizing overexpression or KO system, very few studies elucidate how IPMK levels are modulated under physiological or pathophysiological conditions. However, we have shown that IPMK expression level can be decreased under nutrient deprivation conditions in which ROS is known to increase.[50,72] Hence it is tempting to speculate IPMK can further fine-tune the regulation of Nrf2 under certain conditions, however, these aspects require further investigation. In addition, it is possible that IPMK prevents the overactivation of the Nrf2 signaling pathway under basal conditions, in the absence of stress stimuli. During oxidative stress, the interaction of Nrf2 with IPMK may be decreased. It is also not clear whether IPMK forms a ternary complex with Nrf2 and Keap1. These aspects could be analyzed in future studies. The effect of IPMK on the interaction of Nrf2 with the AREs of target genes *in vivo* is also an area for future investigation, which would further deepen our knowledge of the interaction between the two signaling pathways.

STAR★METHODS

Detailed methods are provided in the online version of this paper and include the following:

- KEY RESOURCES TABLE
- RESOURCE AVAILABILITY
  - Lead contact
  - Materials availability
  - Data and code availability
- EXPERIMENTAL MODELS AND STUDY PARTICIPANT DETAILS
  - Animals
  - Cell culture
- METHOD DETAILS
  - Cell viability assays
  - Cell viability assay in low cysteine and zero cysteine medium
  - Western blotting
  - GST pull down assays
  - Immunoprecipitation analysis
  - Cysteine production assay

- ○ Glutathione measurements
- ○ Quantitative real-time PCR
- ○ PCR array analysis of oxidative stress response genes
- ○ Extraction of nuclear and cytosolic fractions
- **QUANTIFICATION AND STATISTICAL ANALYSIS**

SUPPLEMENTAL INFORMATION

Supplemental information can be found online at https://doi.org/10.1016/j.isci.2023.107199.

AUTHOR CONTRIBUTIONS

B.D.P. conceptualized the study. B.D.P., R.T., S.C., S.J.T., S.F.K., and S.H.S. designed the experiments and analyzed the data. R.T., S.C., S.J.T., I.J., and B.D.P. conducted the experiments. B.D.P., R.T., and S.C. wrote the manuscript with input from all authors.

DECLARATION OF INTERESTS

The authors declare no competing interests.

INCLUSION AND DIVERSITY

We support inclusive, diverse, and equitable conduct of research.

REFERENCES

1. Livermore, T.M., Azevedo, C., Kolozsvari, B., Wilson, M.S.C., and Saiardi, A. (2016). Phosphate, inositol and polyphosphates. Biochem. Soc. Trans. *44*, 253–259. https://doi.org/10.1042/BST20150215.

2. Tu-Sekine, B., and Kim, S.F. (2022). The Inositol Phosphate System-A Coordinator of Metabolic Adaptability. Int. J. Mol. Sci. *23*, 6747. https://doi.org/10.3390/ijms23126747.

3. Frederick, J.P., Mattiske, D., Wofford, J.A., Megosh, L.C., Drake, L.Y., Chiou, S.T., Hogan, B.L.M., and York, J.D. (2005). An essential role for an inositol polyphosphate multikinase, Ipk2, in mouse embryogenesis and second messenger production. Proc. Natl. Acad. Sci. USA *102*, 8454–8459. https://doi.org/10.1073/pnas.0503706102.

4. Saiardi, A., Erdjument-Bromage, H., Snowman, A.M., Tempst, P., and Snyder, S.H. (1999). Synthesis of diphosphoinositol pentakisphosphate by a newly identified family of higher inositol polyphosphate kinases. Curr. Biol. *9*, 1323–1326. https://doi.org/10.1016/s0960-9822(00)80055-x.

5. Odom, A.R., Stahlberg, A., Wente, S.R., and York, J.D. (2000). A role for nuclear inositol 1,4,5-trisphosphate kinase in transcriptional control. Science *287*, 2026–2029. https://doi.org/10.1126/science.287.5460.2026.

6. Leyman, A., Pouillon, V., Bostan, A., Schurmans, S., Erneux, C., and Pesesse, X. (2007). The absence of expression of the three isoenzymes of the inositol 1,4,5-trisphosphate 3-kinase does not prevent the formation of inositol pentakisphosphate and hexakisphosphate in mouse embryonic fibroblasts. Cell. Signal. *19*, 1497–1504. https://doi.org/10.1016/j.cellsig.2007.01.024.

7. Chakraborty, A., Koldobskiy, M.A., Bello, N.T., Maxwell, M., Potter, J.J., Juluri, K.R., Maag, D., Kim, S., Huang, A.S., Dailey, M.J., et al. (2010). Inositol pyrophosphates inhibit Akt signaling, thereby regulating insulin sensitivity and weight gain. Cell *143*, 897–910. https://doi.org/10.1016/j.cell.2010.11.032.

8. Saiardi, A., Bhandari, R., Resnick, A.C., Snowman, A.M., and Snyder, S.H. (2004). Phosphorylation of proteins by inositol pyrophosphates. Science *306*, 2101–2105. https://doi.org/10.1126/science.1103344.

9. Mallery, D.L., Márquez, C.L., McEwan, W.A., Dickson, C.F., Jacques, D.A., Anandapadamanaban, M., Bichel, K., Towers, G.J., Saiardi, A., Böcking, T., and James, L.C. (2018). IP6 is an HIV pocket factor that prevents capsid collapse and promotes DNA synthesis. Elife *7*, e35335. https://doi.org/10.7554/eLife.35335.

10. Wang, H., Falck, J.R., Hall, T.M.T., and Shears, S.B. (2011). Structural basis for an inositol pyrophosphate kinase surmounting phosphate crowding. Nat. Chem. Biol. *8*, 111–116. https://doi.org/10.1038/nchembio.733.

11. Resnick, A.C., Snowman, A.M., Kang, B.N., Hurt, K.J., Snyder, S.H., and Saiardi, A. (2005). Inositol polyphosphate multikinase is a nuclear PI3-kinase with transcriptional regulatory activity. Proc. Natl. Acad. Sci. USA *102*, 12783–12788. https://doi.org/10.1073/pnas.0506184102.

12. Maag, D., Maxwell, M.J., Hardesty, D.A., Boucher, K.L., Choudhari, N., Hanno, A.G., Ma, J.F., Snowman, A.S., Pietropaoli, J.W., Xu, R., et al. (2011). Inositol polyphosphate multikinase is a physiologic PI3-kinase that activates Akt/PKB. Proc. Natl. Acad. Sci. USA *108*, 1391–1396. https://doi.org/10.1073/pnas.1017831108.

13. Cantley, L.C. (2002). The phosphoinositide 3-kinase pathway. Science *296*, 1655–1657.

https://doi.org/10.1126/science.296.5573.1655.

14. Xu, R., Sen, N., Paul, B.D., Snowman, A.M., Rao, F., Vandiver, M.S., Xu, J., and Snyder, S.H. (2013). Inositol polyphosphate multikinase is a coactivator of p53-mediated transcription and cell death. Sci. Signal. 6, ra22. https://doi.org/10.1126/scisignal.2003405.

15. Kim, E., Tyagi, R., Lee, J.Y., Park, J., Kim, Y.R., Beon, J., Chen, P.Y., Cha, J.Y., Snyder, S.H., and Kim, S. (2013). Inositol polyphosphate multikinase is a coactivator for serum response factor-dependent induction of immediate early genes. Proc. Natl. Acad. Sci. USA 110, 19938–19943. https://doi.org/10.1073/pnas.1320171110.

16. Guha, P., Tyagi, R., Chowdhury, S., Reilly, L., Fu, C., Xu, R., Resnick, A.C., and Snyder, S.H. (2019). IPMK Mediates Activation of ULK Signaling and Transcriptional Regulation of Autophagy Linked to Liver Inflammation and Regeneration. Cell Rep. 26, 2692–2703.e7. https://doi.org/10.1016/j.celrep.2019.02.013.

17. Kim, S., Kim, S.F., Maag, D., Maxwell, M.J., Resnick, A.C., Juluri, K.R., Chakraborty, A., Koldobskiy, M.A., Cha, S.H., Barrow, R., et al. (2011). Amino acid signaling to mTOR mediated by inositol polyphosphate multikinase. Cell Metab. 13, 215–221. https://doi.org/10.1016/j.cmet.2011.01.007.

18. Bosch, D., and Saiardi, A. (2012). Arginine transcriptional response does not require inositol phosphate synthesis. J. Biol. Chem. 287, 38347–38355. https://doi.org/10.1074/jbc.M112.384255.

19. Xu, R., Paul, B.D., Smith, D.R., Tyagi, R., Rao, F., Khan, A.B., Blech, D.J., Vandiver, M.S., Harraz, M.M., Guha, P., et al. (2013). Inositol polyphosphate multikinase is a transcriptional coactivator required for immediate early gene induction. Proc. Natl. Acad. Sci. USA 110, 16181–16186. https://doi.org/10.1073/pnas.1315551110.

20. Kim, S., and Snyder, S.H. (2011). Nutrient amino acids signal to mTOR via inositol polyphosphate multikinase. Cell Cycle 10, 1708–1710. https://doi.org/10.4161/cc.10.11.15559.

21. Kim, E., Beon, J., Lee, S., Park, S.J., Ahn, H., Kim, M.G., Park, J.E., Kim, W., Yuk, J.M., Kang, S.J., et al. (2017). Inositol polyphosphate multikinase promotes Toll-like receptor-induced inflammation by stabilizing TRAF6. Sci. Adv. 3, e1602296. https://doi.org/10.1126/sciadv.1602296.

22. Gancedo, C., and Flores, C.L. (2008). Moonlighting proteins in yeasts. Microbiol. Mol. Biol. Rev. 72, 197–210. table of contents. https://doi.org/10.1128/MMBR.00036-07.

23. Ahmed, I., Sbodio, J.I., Harraz, M.M., Tyagi, R., Grima, J.C., Albacarys, L.K., Hubbi, M.E., Xu, R., Kim, S., Paul, B.D., and Snyder, S.H. (2015). Huntington's disease: Neural dysfunction linked to inositol polyphosphate multikinase. Proc. Natl. Acad. Sci. USA 112, 9751–9756. https://doi.org/10.1073/pnas.1511810112.

24. Yokoyama, J.S., Wang, Y., Schork, A.J., Thompson, W.K., Karch, C.M., Cruchaga, C., McEvoy, L.K., Witoelar, A., Chen, C.H., Holland, D., et al. (2016). Association Between Genetic Traits for Immune-Mediated Diseases and Alzheimer Disease. JAMA Neurol. 73, 691–697. https://doi.org/10.1001/jamaneurol.2016.0150.

25. Meister, A. (1983). Selective modification of glutathione metabolism. Science 220, 472–477. https://doi.org/10.1126/science.6836290.

26. Meister, A., and Anderson, M.E. (1983). Glutathione. Annu. Rev. Biochem. 52, 711–760. https://doi.org/10.1146/annurev.bi.52.070183.003431.

27. Dahlin, D.C., Miwa, G.T., Lu, A.Y., and Nelson, S.D. (1984). N-acetyl-p-benzoquinone imine: a cytochrome P-450-mediated oxidation product of acetaminophen. Proc. Natl. Acad. Sci. USA 81, 1327–1331. https://doi.org/10.1073/pnas.81.5.1327.

28. Dimova, S., Hoet, P.H.M., Dinsdale, D., and Nemery, B. (2005). Acetaminophen decreases intracellular glutathione levels and modulates cytokine production in human alveolar macrophages and type II pneumocytes in vitro. Int. J. Biochem. Cell Biol. 37, 1727–1737. https://doi.org/10.1016/j.biocel.2005.03.005.

29. Dimova, S., Hoet, P.H., and Nemery, B. (2000). Paracetamol (acetaminophen) cytotoxicity in rat type II pneumocytes and alveolar macrophages in vitro. Biochem. Pharmacol. 59, 1467–1475. https://doi.org/10.1016/s0006-2952(00)00257-4.

30. Griffith, O.W. (1999). Biologic and pharmacologic regulation of mammalian glutathione synthesis. Free Radic. Biol. Med. 27, 922–935. https://doi.org/10.1016/s0891-5849(99)00176-8.

31. Paul, B.D., Sbodio, J.I., and Snyder, S.H. (2018). Cysteine Metabolism in Neuronal Redox Homeostasis. Trends Pharmacol. Sci. 39, 513–524. https://doi.org/10.1016/j.tips.2018.02.007.

32. McBean, G.J. (2012). The transsulfuration pathway: a source of cysteine for glutathione in astrocytes. Amino Acids 42, 199–205. https://doi.org/10.1007/s00726-011-0864-8.

33. Gaitonde, M.K. (1967). A spectrophotometric method for the direct determination of cysteine in the presence of other naturally occurring amino acids. Biochem. J. 104, 627–633. https://doi.org/10.1042/bj1040627.

34. Sato, H., Tamba, M., Ishii, T., and Bannai, S. (1999). Cloning and expression of a plasma membrane cystine/glutamate exchange transporter composed of two distinct proteins. J. Biol. Chem. 274, 11455–11458. https://doi.org/10.1074/jbc.274.17.11455.

35. Wang, H., Tamba, M., Kimata, M., Sakamoto, K., Bannai, S., and Sato, H. (2003). Expression of the activity of cystine/glutamate exchange transporter, system x(c)(-), by xCT and rBAT. Biochem. Biophys. Res. Commun. 305, 611–618. https://doi.org/10.1016/s0006-291x(03)00808-8.

36. Lewerenz, J., Hewett, S.J., Huang, Y., Lambros, M., Gout, P.W., Kalivas, P.W., Massie, A., Smolders, I., Methner, A., Pergande, M., et al. (2013). The cystine/glutamate antiporter system x(c)(-) in health and disease: from molecular mechanisms to novel therapeutic opportunities. Antioxid. Redox Signal. 18, 522–555. https://doi.org/10.1089/ars.2011.4391.

37. Bannai, S., and Tateishi, N. (1986). Role of membrane transport in metabolism and function of glutathione in mammals. J. Membr. Biol. 89, 1–8. https://doi.org/10.1007/BF01870891.

38. Sbodio, J.I., Snyder, S.H., and Paul, B.D. (2016). Transcriptional control of amino acid homeostasis is disrupted in Huntington's disease. Proc. Natl. Acad. Sci. USA 113, 8843–8848. https://doi.org/10.1073/pnas.1608264113.

39. Itoh, K., Chiba, T., Takahashi, S., Ishii, T., Igarashi, K., Katoh, Y., Oyake, T., Hayashi, N., Satoh, K., Hatayama, I., et al. (1997). An Nrf2/small Maf heterodimer mediates the induction of phase II detoxifying enzyme genes through antioxidant response elements. Biochem. Biophys. Res. Commun. 236, 313–322. https://doi.org/10.1006/bbrc.1997.6943.

40. Baird, L., and Dinkova-Kostova, A.T. (2011). The cytoprotective role of the Keap1-Nrf2 pathway. Arch. Toxicol. 85, 241–272. https://doi.org/10.1007/s00204-011-0674-5.

41. Matsumaru, D., and Motohashi, H. (2020). From germ cells to neonates: the beginning of life and the KEAP1-NRF2 system. J. Biochem. 167, 133–138. https://doi.org/10.1093/jb/mvz070.

42. Deponte, M. (2017). The Incomplete Glutathione Puzzle: Just Guessing at Numbers and Figures? Antioxid. Redox Signal. 27, 1130–1161. https://doi.org/10.1089/ars.2017.7123.

43. Erdélyi, K., Ditrói, T., Johansson, H.J., Czikora, Á., Balog, N., Silwal-Pandit, L., Ida, T., Olasz, J., Hajdú, D., Mátrai, Z., et al. (2021). Reprogrammed transsulfuration promotes basal-like breast tumor progression via realigning cellular cysteine persulfidation. Proc. Natl. Acad. Sci. USA 118, e2100050118. https://doi.org/10.1073/pnas.2100050118.

44. Badgley, M.A., Kremer, D.M., Maurer, H.C., DelGiorno, K.E., Lee, H.J., Purohit, V., Sagalovskiy, I.R., Ma, A., Kapilian, J., Firl, C.E.M., et al. (2020). Cysteine depletion induces pancreatic tumor ferroptosis in mice. Science 368, 85–89. https://doi.org/10.1126/science.aaw9872.

45. Cramer, S.L., Saha, A., Liu, J., Tadi, S., Tiziani, S., Yan, W., Triplett, K., Lamb, C., Alters, S.E., Rowlinson, S., et al. (2017). Systemic depletion of L-cyst(e)ine with cyst(e)inase increases reactive oxygen species and suppresses tumor growth. Nat. Med. 23, 120–127. https://doi.org/10.1038/nm.4232.

46. Fu, C., Tyagi, R., Chin, A.C., Rojas, T., Li, R.J., Guha, P., Bernstein, I.A., Rao, F., Xu, R., Cha, J.Y., et al. (2018). Inositol Polyphosphate Multikinase Inhibits Angiogenesis via Inositol

Pentakisphosphate-Induced HIF-1alpha Degradation. Circ. Res. *122*, 457–472. https://doi.org/10.1161/CIRCRESAHA.117.311983.

47. Coletta, C., Papapetropoulos, A., Erdelyi, K., Olah, G., Módis, K., Panopoulos, P., Asimakopoulou, A., Gerö, D., Sharina, I., Martin, E., and Szabo, C. (2012). Hydrogen sulfide and nitric oxide are mutually dependent in the regulation of angiogenesis and endothelium-dependent vasorelaxation. Proc. Natl. Acad. Sci. USA *109*, 9161–9166. https://doi.org/10.1073/pnas.1202916109.

48. Szabó, C., and Papapetropoulos, A. (2011). Hydrogen sulphide and angiogenesis: mechanisms and applications. Br. J. Pharmacol. *164*, 853–865. https://doi.org/10.1111/j.1476-5381.2010.01191.x.

49. Yang, G., Wu, L., Jiang, B., Yang, W., Qi, J., Cao, K., Meng, Q., Mustafa, A.K., Mu, W., Zhang, S., et al. (2008). H2S as a physiologic vasorelaxant: hypertension in mice with deletion of cystathionine gamma-lyase. Science *322*, 587–590. https://doi.org/10.1126/science.1162667.

50. Bang, S., Kim, S., Dailey, M.J., Chen, Y., Moran, T.H., Snyder, S.H., and Kim, S.F. (2012). AMP-activated protein kinase is physiologically regulated by inositol polyphosphate multikinase. Proc. Natl. Acad. Sci. USA *109*, 616–620. https://doi.org/10.1073/pnas.1119751109.

51. Li, Y., Liu, M., Song, X., Zheng, X., Yi, J., Liu, D., Wang, S., Chu, C., and Yang, J. (2020). Exogenous Hydrogen Sulfide Ameliorates Diabetic Myocardial Fibrosis by Inhibiting Cell Aging Through SIRT6/AMPK Autophagy. Front. Pharmacol. *11*, 1150. https://doi.org/10.3389/fphar.2020.01150.

52. Calvert, J.W., Jha, S., Gundewar, S., Elrod, J.W., Ramachandran, A., Pattillo, C.B., Kevil, C.G., and Lefer, D.J. (2009). Hydrogen sulfide mediates cardioprotection through Nrf2 signaling. Circ. Res. *105*, 365–374. https://doi.org/10.1161/CIRCRESAHA.109.199919.

53. Yang, G., Zhao, K., Ju, Y., Mani, S., Cao, Q., Puukila, S., Khaper, N., Wu, L., and Wang, R. (2013). Hydrogen sulfide protects against cellular senescence via S-sulfhydration of Keap1 and activation of Nrf2. Antioxid. Redox Signal. *18*, 1906–1919. https://doi.org/10.1089/ars.2012.4645.

54. Gu, C., Stashko, M.A., Puhl-Rubio, A.C., Chakraborty, M., Chakraborty, A., Frye, S.V., Pearce, K.H., Wang, X., Shears, S.B., and Wang, H. (2019). Inhibition of Inositol Polyphosphate Kinases by Quercetin and Related Flavonoids: A Structure-Activity Analysis. J. Med. Chem. *62*, 1443–1454. https://doi.org/10.1021/acs.jmedchem.8b01593.

55. Faraonio, R., Vergara, P., Di Marzo, D., Pierantoni, M.G., Napolitano, M., Russo, T., and Cimino, F. (2006). p53 suppresses the Nrf2-dependent transcription of antioxidant response genes. J. Biol. Chem. *281*, 39776–39784. https://doi.org/10.1074/jbc.M605707200.

56. Yamamoto, M., Kensler, T.W., and Motohashi, H. (2018). The KEAP1-NRF2 System: a Thiol-Based Sensor-Effector Apparatus for Maintaining Redox Homeostasis. Physiol. Rev. *98*, 1169–1203. https://doi.org/10.1152/physrev.00023.2017.

57. Itoh, K., Wakabayashi, N., Katoh, Y., Ishii, T., Igarashi, K., Engel, J.D., and Yamamoto, M. (1999). Keap1 represses nuclear activation of antioxidant responsive elements by Nrf2 through binding to the amino-terminal Neh2 domain. Genes Dev. *13*, 76–86. https://doi.org/10.1101/gad.13.1.76.

58. Kobayashi, A., Kang, M.I., Okawa, H., Ohtsuji, M., Zenke, Y., Chiba, T., Igarashi, K., and Yamamoto, M. (2004). Oxidative stress sensor Keap1 functions as an adaptor for Cul3-based E3 ligase to regulate proteasomal degradation of Nrf2. Mol. Cell Biol. *24*, 7130–7139. https://doi.org/10.1128/MCB.24.16.7130-7139.2004.

59. Ishii, T., Itoh, K., Takahashi, S., Sato, H., Yanagawa, T., Katoh, Y., Bannai, S., and Yamamoto, M. (2000). Transcription factor Nrf2 coordinately regulates a group of oxidative stress-inducible genes in macrophages. J. Biol. Chem. *275*, 16023–16029. https://doi.org/10.1074/jbc.275.21.16023.

60. Meyer, R., Nalaskowski, M.M., Ehm, P., Schröder, J., Naj, X., Brehm, M.A., and Mayr, G.W. (2012). Nucleocytoplasmic shuttling of human inositol phosphate multikinase is influenced by CK2 phosphorylation. Biol. Chem. *393*, 149–160. https://doi.org/10.1515/hsz-2011-0209.

61. Sedlak, T.W., Paul, B.D., Parker, G.M., Hester, L.D., Snowman, A.M., Taniguchi, Y., Kamiya, A., Snyder, S.H., and Sawa, A. (2019). The glutathione cycle shapes synaptic glutamate activity. Proc. Natl. Acad. Sci. USA *116*, 2701–2706. https://doi.org/10.1073/pnas.1817885116.

62. Wang, A.M., Pradhan, S., Coughlin, J.M., Trivedi, A., DuBois, S.L., Crawford, J.L., Sedlak, T.W., Nucifora, F.C., Jr., Nestadt, G., Nucifora, L.G., et al. (2019). Assessing Brain Metabolism With 7-T Proton Magnetic Resonance Spectroscopy in Patients With First-Episode Psychosis. JAMA Psychiatr. *76*, 314–323. https://doi.org/10.1001/jamapsychiatry.2018.3637.

63. Sedlak, T.W., Nucifora, L.G., Koga, M., Shaffer, L.S., Higgs, C., Tanaka, T., Wang, A.M., Coughlin, J.M., Barker, P.B., Fahey, J.W., and Sawa, A. (2018). Sulforaphane Augments Glutathione and Influences Brain Metabolites in Human Subjects: A Clinical Pilot Study. Mol. Neuropsychiatry *3*, 214–222. https://doi.org/10.1159/000487639.

64. Niwa, M., Jaaro-Peled, H., Tankou, S., Seshadri, S., Hikida, T., Matsumoto, Y., Cascella, N.G., Kano, S.i., Ozaki, N., Nabeshima, T., and Sawa, A. (2013). Adolescent stress-induced epigenetic control of dopaminergic neurons via glucocorticoids. Science *339*, 335–339. https://doi.org/10.1126/science.1226931.

65. Kubben, N., Zhang, W., Wang, L., Voss, T.C., Yang, J., Qu, J., Liu, G.H., and Misteli, T. (2016). Repression of the Antioxidant NRF2 Pathway in Premature Aging. Cell *165*, 1361–1374. https://doi.org/10.1016/j.cell.2016.05.017.

66. Paul, B.D., Sbodio, J.I., Xu, R., Vandiver, M.S., Cha, J.Y., Snowman, A.M., and Snyder, S.H. (2014). Cystathionine gamma-lyase deficiency mediates neurodegeneration in Huntington's disease. Nature *509*, 96–100. https://doi.org/10.1038/nature13136.

67. Paul, B.D. (2021). Neuroprotective Roles of the Reverse Transsulfuration Pathway in Alzheimer's Disease. Front. Aging Neurosci. *13*, 659402. https://doi.org/10.3389/fnagi.2021.659402.

68. Paul, B.D., Sbodio, J.I., and Snyder, S.H. (2022). Mutant Huntingtin Derails Cysteine Metabolism in Huntington's Disease at Both Transcriptional and Post-Translational Levels. Antioxidants *11*, 1470. https://doi.org/10.3390/antiox11081470.

69. Paul, B.D., Lemle, M.D., Komaroff, A.L., and Snyder, S.H. (2021). Redox imbalance links COVID-19 and myalgic encephalomyelitis/chronic fatigue syndrome. Proc. Natl. Acad. Sci. USA *118*, e2024358118. https://doi.org/10.1073/pnas.2024358118.

70. Wang, Z., Wu, P., Shi, J., Ji, X., He, L., Dong, W., Wang, Z., Zhang, H., and Sun, W. (2022). A novel necroptosis-related gene signature associated with immune landscape for predicting the prognosis of papillary thyroid cancer. Front. Genet. *13*, 947216. https://doi.org/10.3389/fgene.2022.947216.

71. Ziros, P.G., Manolakou, S.D., Habeos, I.G., Lilis, I., Chartoumpekis, D.V., Koika, V., Soares, P., Kyriazopoulou, V.E., Scopa, C.D., Papachristou, D.J., and Sykiotis, G.P. (2013). Nrf2 is commonly activated in papillary thyroid carcinoma, and it controls antioxidant transcriptional responses and viability of cancer cells. J. Clin. Endocrinol. Metab. *98*, E1422–E1427. https://doi.org/10.1210/jc.2013-1510.

72. Jung, I.R., Anokye-Danso, F., Jin, S., Ahima, R.S., and Kim, S.F. (2022). IPMK modulates hepatic glucose production and insulin signaling. J. Cell. Physiol. *237*, 3421–3432. https://doi.org/10.1002/jcp.30827.

73. Furukawa, M., and Xiong, Y. (2005). BTB protein Keap1 targets antioxidant transcription factor Nrf2 for ubiquitination by the Cullin 3-Roc1 ligase. Mol. Cell. Biol. *25*, 162–171. https://doi.org/10.1128/MCB.25.1.162-171.2005.

STAR★METHODS

KEY RESOURCES TABLE

REAGENT or RESOURCE	SOURCE	IDENTIFIER
Antibodies		
Mouse IgG, HRP-linked whole Ab (from sheep) (1:3000)	Millipore Sigma	Cat#NA931-1ML, RRID: N/A
Rabbit IgG, HRP-linked whole Ab (from donkey) (1:3000)	Millipore Sigma	Cat#NA934-1ML, RRID: N/A
Anti-Actin HRP (1: 3000)	Santa Cruz Biotechnology	Cat# sc-47778, RRID:AB_626632 HRP
Anti-CSE (1:3000)	Snyder Lab[49]	N/A
Anti-GFP (1:1000)	Cell Signaling	Cat# 2956, RRID:AB_1196615
Anti-GCLC (1: 1000)	Santa Cruz Biotechnology	Cat# sc-166356, RRID:AB_2107820
Anti-GSTA2 (1:1000)	Proteintech	Cat# 10505-1-AP, RRID:AB_2248094
Anti-H2B (1:1000)	Cell Signaling	Cat# 8135, RRID:AB_10891053
Anti-Heme Oxygenase 1 Antibody (H-105)	Santa Cruz Biotechnology	Cat# sc-10789, RRID:AB_648281
Anti-IPMK (1:3000)	Dr. Sangwon F. Kim, Johns Hopkins University	N/A
Anti-IPMK (1:1000)	Novus Biologicals	Cat# NBP1-32250, RRID:AB_2127660
Anti-LDH (1:1000)	Cell Signaling	Cat# 2012, RRID:AB_2137173
Anti-Nrf2 (1:100)	Cell Signaling	Cat# 12721, RRID:AB_2715528
Anti-xCT (SLC7A11) (1:1000)	Abcam	Cat# ab37185, RRID:AB_778944
Chemicals, peptides, and recombinant proteins		
L-Cystathionine	Millipore Sigma	C7505
L-Cysteine	Sigma	N5514
Dimethyl sulfoxide, >=99.9% A.C.S. REAGENT, DMSO	Sigma Aldrich	472301-4L
Dulbecco's Modified Eagle Medium (DMEM)	Thermo Fisher Scientific	11965-092
DMEM, high glucose, no glutamine, no methionine, no cystine	Thermo Fisher Scientific	21013024
Erastin	Cayman Chemicals	17754
Fetal bovine serum	Gemini	50-753-2981
L-Glutamine (2 mM)	Invitrogen	25030-081
Glutathione Sepharose® 4B Cytiva 17-0756-01, pack of 10 mL	Millipore Sigma	GE17-0756-01
Hydrochloric acid 36.5-38.0%, BioReagent, for molecular biology	Millipore Sigma	H1758
Hydrogen peroxide (H_2O_2)	Sigma	H1009
Lipofectamine™ 3000 Transfection Reagent	ThermoFisher Scientific	L3000150
Methionine	Millipore Sigma	M0960000
Methylthiazoletetrazolium (MTT)	Thermo Fisher Scientific	M6494
Ninhydrin	Sigma Aldrich	N4876
Nuclease free water	Ambion	AM993
Opti-MEM® I Reduced Serum Medium	Thermo Fisher Scientific	31985070
Propidium Iodide	Invitrogen ReadyProbes™ Reagent	R37108
Protease Inhibitor: cOmplete™, Mini, EDTA-free Protease Inhibitor Cocktail	Millipore Sigma	4693159001
Protein A/G agarose	Calbiochem	IP05-1.5ML
PVDF Immobilon-FL membrane	EMD Millipore	IPFL00010

Continued

REAGENT or RESOURCE	SOURCE	IDENTIFIER
Pyridoxal 5′-phosphate hydrate	Sigma Aldrich	P9255
Pyrogallol	Sigma	83130
SuperSignal™ West Pico PLUS Chemiluminescent Substrate	ThermoFisher Scientific	34580
Trypan Blue	Invitrogen, Life Technologies	T10282
Trypsin-EDTA (0.05%)	Gibco	25300-054
Critical commercial assays		
Mouse RT2 Profiler™ PCR Array	Qiagen	PAMM-065Z, 330231
Nuclear –Cytoplasmic fractionation kit	Biovision	K266-25
Promega GSH/GSSG-Glo™ Glutathione Assay	Promega	V6612
Protein Assay Dye Reagent	Biorad	22660
RNeasy Plus Universal Kit	Qiagen	73404
RNeasy Plus Mini Kit (50)	Qiagen	74134
RT^2 First Strand Kit	Qiagen	330401
RT^2 SYBR Green ROX qPCR Mastermix	Qiagen	330520
TaqMan RNA-to-C_t 1-Step Kit	Life Technologies	4392653
Experimental models: Cell lines		
$IPMK^{-/-}$ mouse embryonic fibroblasts	Xu et al., 2013b	N/A
HEK293	American Type Culture Collection (ATCC)	ATCC Cat# CRL-1573, RRID:CVCL_0045
Experimental models: Organisms/strains		
$IPMK^{-/-}$ Alb Cre mouse model and their wild type controls	Dr. Sangwon F. Kim, Johns Hopkins University	N/A
Albumin-CreTg/+ mice (B6.Cg-Speer6-ps1$^{Tg(Alb-cre)21Mgn}$/J)	Jackson Laboratories	strain number: 003574, RRID:IMSR_JAX:003574
Oligonucleotides		
TaqMan® Gene Expression Assay, Gene Symbol:Prdx2, Dye Label and Assay Concentration: FAM-MGB / 20X	Life Technologies	Assay ID: Mm00448996_m1
TaqMan® Gene Expression Assay, Gene Symbol: Gclc, Dye Label and Assay Concentration: FAM-MGB / 20X	Life Technologies	Assay ID: Mm00802655_m1
TaqMan® Gene Expression Assay, Gene Symbol: Gclm, Dye Label and Assay Concentration: FAM-MGB / 20X	Life Technologies	Assay ID: Mm01324400_m1
TaqMan® Gene Expression Assay, Gene Symbol: GstA2, Dye Label and Assay Concentration: FAM-MGB / 20X	Life Technologies	Assay ID: Mm00833353_mH
TaqMan® Gene Expression Assay, Gene Symbol: Fth1, Dye Label and Assay Concentration: FAM-MGB / 20X	Life Technologies	Assay ID: Mm04336018_m1
TaqMan® Gene Expression Assay, Gene Symbol: Hmox1, Dye Label and Assay Concentration: FAM-MGB / 20X	Life Technologies	Assay ID: Mm00802655_m1
TaqMan® Gene Expression Assay, Gene Symbol: Txrnd1, Dye Label and Assay Concentration: FAM-MGB / 20X	Life Technologies	Assay ID: Mm00443675_m1
TaqMan® Gene Expression Assay, Gene Symbol: Txrnd2, Dye Label and Assay Concentration: FAM-MGB / 20X	Life Technologies	Assay ID: Mm00496766_m1
TaqMan® Gene Expression Assay, Gene Symbol: Cth, Dye Label and Assay Concentration: FAM-MGB / 20X	Life Technologies	Assay ID: Mm00461247_m1
TaqMan® Gene Expression Assay, Gene Symbol: Ipmk, Dye Label and Assay Concentration: FAM-MGB / 20X	Life Technologies	Assay ID: Mm01148672_m1
TaqMan® Gene Expression Assay, Gene Symbol: Nqo1, Dye Label and Assay Concentration: FAM-MGB / 20X	Life Technologies	Assay ID: Mm01253561_m1

Continued

REAGENT or RESOURCE	SOURCE	IDENTIFIER
TaqMan® Gene Expression Assay, Gene Symbol: *Pgd*, Dye Label and Assay Concentration: FAM-MGB / 20X	Life Technologies	Assay ID: Mm00503037_m1
TaqMan® Gene Expression Assay, Gene Symbol: *Gpx1*, Dye Label and Assay Concentration: FAM-MGB / 20X	Life Technologies	Assay ID: Mm00656767_g1
TaqMan® Gene Expression Assay, Gene Symbol: *Gpx2*, Dye Label and Assay Concentration: FAM-MGB / 20X	Life Technologies	Assay ID: Mm00850074_g1
TaqMan® Gene Expression Assay, Gene Symbol: *Tuba1a*, Dye Label and Assay Concentration: FAM-MGB / 20X	Life Technologies	Assay ID: Mm00846967_g1
TaqMan® Gene Expression Assay, Gene Symbol: *Gpx7*, Dye Label and Assay Concentration: FAM-MGB / 20X	Life Technologies	Assay ID: Mm00481133_m1
Recombinant DNA		
Plasmid: GST-IPMK constructs	Snyder Lab[17]	N/A
Plasmid: GFP-Nrf2	Addgene[73]	RRID:Addgene_21549
Software and algorithms		
GraphPad Prism	GraphPad Software, Inc	graphpad.com
Image J	NIH	https://imagej.net/ij/index.html
Biorender	Biorender	https://www.biorender.com

RESOURCE AVAILABILITY

Lead contact

Further information and requests for resources and reagents should be directed to and will be fulfilled by the lead contact, Bindu Paul (bpaul8@jhmi.edu).

Materials availability

Plasmids and mouse lines generated in this study are available from the lead contact upon reasonable request with a completed Materials Transfer Agreement.

Data and code availability

- All data reported in this paper will be shared by the lead contact upon request.
- This paper does not report the original code.
- Any additional information required to reanalyze the data reported in this paper is available from the lead contact upon request.

EXPERIMENTAL MODELS AND STUDY PARTICIPANT DETAILS

Animals

The study protocol was approved by the Institutional Animal Care and Use Committee of Johns Hopkins University. All animal procedures were performed in accordance with the National Institutes of Health guidelines (Guide for the Care and Use of Laboratory Animals). The liver-specific $IPMK^{-/-}$ (IPMK-LKO) mice were generated by crossing Albumin-CreTg/+ mice (strain number: 003574, Albumin-CreTg/+ mice (B6.Cg-*Speer6-ps1*$^{Tg(Alb-cre)21Mgn}$/J, Jackson Laboratories) with mice homozygous for a "floxed" allele of exon 6 of IPMK (IPMK *fl//fl*). The control mice for this study were IPMK *fl/fl* (wild type [WT]) mice. Mouse were grouped-housed in individually ventilated cages with five mice per cage. Corn cob was used as bedding and nestlets were provided as nesting material. All the mice were maintained in a controlled environment at a temperature of 22°C +/- 1°C, with a light–dark cycle of 12 h (lights on at 07:00) and provided with a normal chow diet (containing 13% fat, 23.3% protein, and 63.7% carbohydrate; LabDiet) and water *ad libitum*. Healthy WT and IPMK-LKO naïve male mice aged 8 months were randomly assigned to experimental groups and used for quantitative real-time PCR analysis.

Cell culture

MEFs from both wild-type and IPMK$^{-/-}$ mice were generated in laboratory as reported earlier.[12] All cell lines used in this study were cultured in Dulbecco's Modified Eagle Medium (DMEM; Invitrogen) supplemented with 10% fetal bovine serum, L-Glutamine (2 mM; Invitrogen) and penicillin/streptomycin (Invitrogen) at 37°C in a 5% CO2 humidified atmosphere.

For rescue experiments, control myc, wild-type myc-IPMK, kinase-dead myc-IPMK constructs were cloned into pMXS vector containing blasticidin resistance. These plasmids were transfected into *IPMK$^{-/-}$* MEFs cells and selected with 5 μg/mL blasticidin resistance. These stably transfected cell lines were maintained in 5 μg/mL blasticidin supplemented DMEM. The *IPMK$^{-/-}$* and the *IPMK fl//fl* cell lines used in the study are routinely validated by genotyping and western blot analysis.

METHOD DETAILS

Cell viability assays

MTT assay

Prior to the treatments MEFs were plated at a density of 1.5 x 10^5 cells per well in a 24-well plate. After being allowed to attach for 8 hours, cells were treated with H$_2$O$_2$, pyrogallol, sulfasalazine, or acetaminophen for 16 hours. Subsequently, media was replaced with fresh media containing 0.5 mg/ml MTT for 1 hour. The media was removed, and cells were lysed in DMSO to dissolve the reduced cellular MTT. Cell viability was calculated by measuring the absorbance at 570 nm, using 630 nm as the reference for cell debris.

Propidium iodide assay

Propidium iodide assay was used to quantify cell death and performed using the Propidium Iodide ReadyProbes™ Reagent (Invitrogen, Life Technologies, Carlsbad, CA) according to the manufacturer's instructions. After growing the cells in regular or no cysteine media, cells were stained with two drops of Propidium iodide per mL of the culture medium and incubated for 15 minutes at 37°C. Cells were harvested, and the number of propidium iodide-stained cells was counted using a Countess® Automated Cell Counter (Invitrogen, Life Technologies, USA).

Trypan blue staining

Briefly, after the growth of cells in regular or no cysteine media, cells were trypsinized, centrifuged, and re-suspended in regular media. Then, 10 μl of the sample was mixed with 10 μl trypan blue and loaded onto the Countess chamber slide. The cell viability was estimated using a cell counter (Countess®, ThermoFisher Scientific).

Cell viability assay in low cysteine and zero cysteine medium

The low-cysteine medium was prepared from the minus cysteine and minus methionine media (Life Technologies). Methionine was added at a concentration of 0.2 mM, and cysteine was added at a concentration of 0.05 mM. For the total cysteine deprivation assay, cysteine was not supplemented. MEFs were plated at a density of 2 x 10^4 cells per well in 96 well plate. 8 hours post plating MEFs were kept in low cysteine media for 24 hours. Cell viability assays were performed using RealTime-Glo MT Cell Viability Assay kit (Promega).

Western blotting

Cells were lysed on ice for 20 min in lysis buffer (also IP buffer) containing 50 mM Tris-HCl pH 8.0, 150 mM NaCl, 1% Triton X-100, protease inhibitors (cOmplete™, EDTA-free Protease Inhibitor Cocktail from Sigma) and protein phosphatase inhibitor cocktail. Lysates were centrifuged at 16,000 g for 15 min followed by recovery of the supernatant. Lysates were normalized for total protein content using Protein Assay Dye Reagent (Bio-Rad). Protein samples were prepared by adding 1X final concentration of NuPAGE LDS Sample Buffer (Invitrogen) followed by incubation at 95°C for 5 min. Subsequently, protein samples were resolved on a mini NuPAGE 4-12% Bis-Tris gel (Thermo Fisher, Scientific USA) in the presence of 1X NuPAGE MES SDS running buffer (Thermo Fisher, Scientific USA). Proteins were then transferred to Immobilon-FL (Millipore). Membranes were blocked for 1 hour at room temperature with 5% BSA or 5% milk in TBS followed by incubation with the indicated primary antibodies. Horse peroxidase-conjugated secondary antibodies were used for detection with SuperSignal West Pico chemiluminescence reagent (Thermo Fisher, Scientific USA).

GST pull down assays

HEK293 cells were transfected with indicated plasmids for 24 h. Cells were lysed in buffer (IP buffer) and lysates were cleared by centrifugation at 16,000 g for 15 min followed by recovery of the supernatant. Protein was quantified by Bradford assay (Biorad) and samples were normalized for protein content. Inputs were reserved and 500 μg of protein was incubated with glutathione sepharose beads overnight at 4°C with rotation. Beads were washed four times in IP buffer, followed by elution into 1X LDS buffer (Stock 4X containing 40% glycerol, 4% lithium dodecyl sulfate (LDS), 0.8 M triethanolamine-Cl pH 7.6, 4% Ficoll®-400, 0.025% phenol red, 0.025% Coomassie G250, 2 mM EDTA disodium from Thermo Fisher Scientific, USA) with 1 mM DTT at 95°C for 5 min. Samples and inputs were loaded on a mini NuPAGE 4-12% Bis-Tris gel (ThermoFisher, Scientific USA) and electrophoresed in 1X NuPAGE MES (2-(N-morpholino) ethanesulfonic acid) SDS running buffer (ThermoFisher Scientific, USA) and immunoblotted with the indicated antibodies.

Immunoprecipitation analysis

For the *in vivo* immunoprecipitation assays, 500 μg of liver lysates in 1mL of IP buffer were incubated with anti-Nrf2 antibody or normal mouse IgG control was incubated overnight at 4°C with rotation. Protein A/G agarose (Calbiochem, San Diego, CA, USA) was added to the lysates the next day for 2 h and beads collected by centrifugation. Beads were washed four times in IP buffer followed by elution into 30 μL of 1X LDS buffer with 1 mM DTT at 95°C for 5 min. Samples were centrifuged for 3 min at $16,000 \times g$, and supernatant was loaded. Samples and inputs were analyzed by western blotting as described above. Additional details of reagents and methods are provided in the resources section.

Cysteine production assay

Cysteine formed by CSE was quantified as described previously.[33] Ninhydrin reagent was prepared by dissolving 250 mg of ninhydrin in 6 ml of glacial acetic acid and 4 mL of 12 M HCl. Samples (200 μL) were mixed with 60 μL of 6% perchloric acid, and precipitated protein was removed by centrifugation. Next, 200 μL of the supernatant was mixed with 200 μLof glacial acetic acid and ninhydrin, then boiled for 10 min, cooled on ice and mixed with 95% ethanol to a final volume of 1 mL. The absorbance was measured at 560 nm.

Glutathione measurements

Total glutathione (GSH+GSSG) and oxidized glutathione (GSSG) were measured using GSH/GSSG-Glo Assay kit (Promega) as per manufacturer's instructions. Briefly, MEFs were plated at a density of 10,000 cells per well on a flat bottom, tissue culture-treated white-with-clear-bottom 96 well plate. Following day, culture media was removed, and cells were lysed either with 50 μL of Total or Oxidized Glutathione Reagent for 5 min at room temperature. 50 μL Luciferin Generation reagent was added to each well followed by 30 min incubation at room temperature. Then, 100 μL of Luciferin Detection Reagent was added to each well. Finally, luminescence was measured using a plate reader.

Quantitative real-time PCR

Total RNA from liver tissue was isolated from WT or liver-specific knock outs of IPMK mice using TRIzol reagent (Thermo Fisher Scientific), and purified using the RNeasy Plus Universal Kit, and quantified using a Nanodrop Spectrophotometer (Life Technologies). 20 ng of total RNA was used for qPCR using Taqman probes and the TaqMan RNA-to-C_t 1-Step Kit as per the manufacturers's recommendations and the Step One Plus thermocycler (Life Technologies).

PCR array analysis of oxidative stress response genes

RNA isolation and cDNA synthesis. The total RNA from MEFs was extracted and purified using the RNeasy Mini Kit (Qiagen, Valencia, CA, USA) and converted to cDNA using the RT2 First Strand Kit (Qiagen, Valencia, CA, USA). The quantity and quality of the RNA extracts were quantified using a NanoDrop® ND-1000 Spectrophotometer (Thermo Scientific Inc, Waltham, MA) at 260/280 nm ratios. Only high-quality RNA with 260/280 nm ratios of 1.8 to 2.0 and concentrations greater than 40 μg/mL were used for PCR analysis.

Mouse RT2 Profiler™ PCR Array (Cat. No: PARN-065Z, SABiosciences—Qiagen, Valencia, CA, USA) profiling the expression of 84 genes related to oxidative stress, ROS metabolism and related oxygen transporter genes was used for analysis of oxidative stress specific transcripts following the manufacturer's guidelines. Each array contained primers for 84 pathway-related genes and five housekeeping genes,

and 7 wells included reverse-transcription controls, positive PCR controls, and a genomic DNA contamination control. Briefly, 1248 μL nuclease-free water (AM9937, Ambion, USA), 1350 μL SYBR green (ABI) and 102 μL cDNA were mixed in a solution. A total of 25 μL was added to each well of the 96-well array plate from this solution. This plate was briefly spun for 20 s at 1400 rpm. Amplification conditions were set at 95°C for 10 mins for activation of HotStart DNA Taq polymerase. Then 40 cycles were performed at 95°C for 15 s and 60°C (annealing) for 1 min. The Applied Biosystems StepOnePlus was used for RT-PCR.

Data analysis was done based on the $2-\Delta\Delta Ct$ values. Fold change values for each gene were tabulated and further analyzed using Qiagen's web-based PCR Array data analysis software (http://pcrdataanalysis.sabiosciences.com/pcr/arrayanalysis.php). This tool provided a quality check step followed by normalization of data with housekeeping genes (*Actb, B2m, Hprt1, Ldha* and *Rplp1*) and then determination of statistically significant up- or downregulated genes (fold change values greater than 2 or less than 0.5). Only Ct values <35 were included in the calculations.

Extraction of nuclear and cytosolic fractions

The nuclear and cytosolic fractions from HEK-293 cells were collected using a nuclear and cytosol extraction kit (K266, Biovision). Briefly, following transfection with GST vector or GST-IPMK, cells were collected by centrifugation and resuspended in 0.2 ml of cytosol extraction buffer A containing DTT and protease inhibitor. Cytosolic fraction was extracted with extraction buffer B following centrifugation. The pellet was resuspended in nuclear extraction buffer, vortexed, and centrifuged to obtain a nuclear fraction. These fractions were later used to evaluate the effect of IPMK on the compartmentalization of GFP-Nrf2.

QUANTIFICATION AND STATISTICAL ANALYSIS

Statistical analyses were performed using Microsoft Excel 2010 and GraphPad Prism 8 software (GraphPad Software). Statistical significance was determined by either Student's t-test (two-tailed), Two-way ANOVA or One-way ANOVA. Differences between the groups were analyzed using Tukey's post-hoc test. A value of $P < 0.05$ was considered statistically significant. Data are presented as means $\pm$ standard errors of the mean (SEMs) and n indicates the number of biological replicates or the number of animals utilized for experiment.